

The influence of cellulose nanocrystals on the microstructure of cement paste

Yizheng Cao; Nannan Tian; David Bahr; Pablo D Zavattieri; Jeffrey Youngblood; Robert J Moon; Jason Weiss

Abstract

This paper reports the influence of raw and sonicated cellulose nanocrystals (CNCs) on the microstructure of cement paste. A novel centrifugation method is designed to measure the concentrations of the adsorbed CNCs (aCNCs) on the cement surface, and the free CNCs (fCNCs) which are mobile in water. It is found that, the majority of the CNCs (>94%) are aCNCs. More importantly, sonication does not significantly reduce the amount of aCNCs (reduction of less than 2%). We surmise that, after sonication, the aCNCs are primarily dispersed over the cement surface, instead of becoming fCNCs via sonication. Isothermal calorimetry and energy-dispersive X-ray spectroscopy (EDX) results support this theory. The water desorption tests show that the total porosities of cement pastes with raw and sonicated CNCs are 14.8% and 14.4%, which showed a reduction from 16% for the plain cement paste. The porosity reduction is a result of an increase in the degree of hydration. The advantage of sonicated CNCs is they are dispersed, avoiding therefore agglomerates that can lead to pores, voids, and air entrapment. The nanoindentation results show that the reduced indentation modulus on the interfacial regions between cement particles and the low density CSH is increased when CNCs are used.

Keywords

cellulose nanocrystal, cement, agglomeration, ultrasonication, flexural strength, nanoindentation

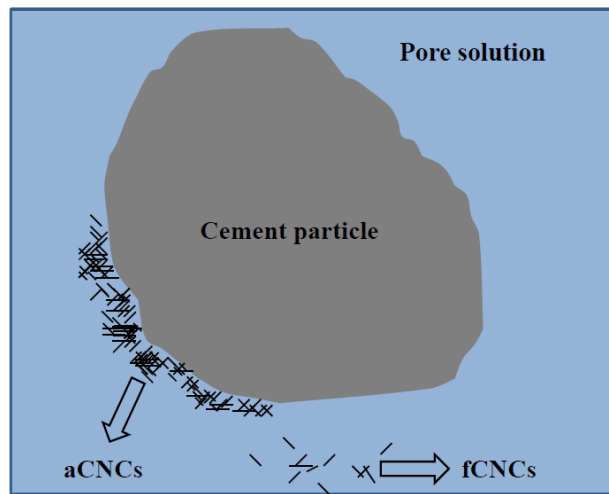
1. Introduction

Cellulose nanocrystal (CNC) is the crystalline part of the cellulose materials, which can be extracted from trees and a variety of plants [1]. As a reinforcement material, CNC has a few extraordinary advantages, including biodegradability, high abundance, low cost, and excellent mechanical properties [1]. Recently, CNCs have been found to improve the flexural strength of cement composites due to an increase in the degree of hydration (DOH) [2] which is possibly aided by a mechanism referred to as short circuit diffusion (SCD). The basic prerequisite for SCD is the adsorption of CNCs on the surface of cement particles, acting as the pathway to preferentially transport water from pores to unhydrated cement cores. Such capability can be attributed to the high hydrophilicity and hygroscopicity of the CNCs [3]. A competing mechanism has also been identified for CNC concentrations larger than 0.2 vol. % where agglomerates induce stress concentrators limiting the strength of the cement pastes [2]. This issue was

34 subsequently addressed by Cao et al. [4] with ultrasonication (or sonication) to disperse the CNCs in the
35 aqueous suspension before mixing with cement.

36
37 The concentration of the CNCs adsorbed on the cement particles is an important factor as it directly
38 influences the SCD. For simplicity the CNCs in the fresh cement paste are categorized as two types: the
39 “free” CNCs in the water and the “adsorbed” CNCs on cement surface (abbreviated as fCNCs and aCNCs,
40 respectively) as illustrated in Fig. 1. While both types of CNCs are in solution, the main difference is that
41 the aCNCs are hard to move, as they adhere to the cement particles and the fCNCs can freely move in the
42 aqueous suspension. The classification and quantification of these two types of CNCs are important for
43 four reasons: we hypothesize that (1) the SCD is primarily governed by the amount of aCNCs; and (2) the
44 strength of the cement is largely limited by the CNC agglomeration; we also lack sufficient information
45 about (3) the role the fCNCs on the cement properties; (4) the mobility of CNCs in the cement paste. We
46 present a novel experimental approach to measure the concentrations aCNCs and fCNCs and their effect
47 on SCD.

48



49

50 Fig. 1. The schematic of the two different types of CNCs in the fresh cement paste

51

52 This paper focuses on the characterization of the cement pastes with raw and sonicated CNCs at the
53 micro-level and studies how the dispersion of CNCs influences the microstructures of cement paste. A
54 novel centrifugation experiment is designed to study the influence of sonication on the concentrations of
55 fCNCs and aCNCs in the fresh cement paste. In addition, isothermal calorimetry is performed to provide
56 the information on cement hydration with sonicated CNCs. For the hardened cement pastes (age of 28
57 days), nanoindentation is used to study how CNCs influence the elastic modulus and hardness of the three
58 phases: unhydrated cement, interfacial region, and the low density CSH. In addition, SEM and EDX are

59 employed to characterize the distribution of CNCs in the cement paste. Finally the water desorption test is
 60 used on the hardened cement pastes to study pore size distribution and how CNCs reduce the pores.

61

62 **2. Materials and experimental testing**

63 **2.1. Materials**

64 A Type V cement was used in this investigation due to its compositional purity (i.e., low aluminates and
 65 ferrite phases), the Bogue compositions and Blaine fineness of which are shown in Table 1.

66

67 Table 1. Bogue compositions of Type V cement

C ₃ S (%)	63.8
C ₂ S (%)	13
C ₃ A (%)	0
C ₄ AF+C ₂ F (%)	12.6
Blaine fineness, m ² /kg	316

68

69 The CNC materials used in this work were manufactured and provided by the USDA Forest Service-
 70 Forest Products Laboratory, Madison, WI, (FPL) [5]. The as-received CNC materials were in a form of
 71 freeze dried powders, 0.96 wt. % sulfur on CNC. The CNCs were extracted using sulfuric acid hydrolysis
 72 of Eucalyptus dry-lap cellulose fibers, resulting in a 0.81 wt. % CNC surface-grafted sulfate content.

73

74 **2.2. Cement paste preparation**

75 For cement past preparation, cement is added to the mixing container, then CNCs are added to the cement
 76 powder, and the final step is to add water to keep the water to cement ratio (w/c) at 0.35. The mixing
 77 procedures are described in the previous work [2] and the mixtures proportions are listed in Table 2.

78

79 Table 2. Experimental matrix for cement pastes with CNCs

Mixture ID	wt (g)			vol (cm ³)			CNC/cement vol %
	cement	CNC	water	cement	CNC	water	
1 (ref)	500	0	175	160.3	0	175	0.00%
2	500	0.103	175	160.3	0.064	175	0.04%
3	500	0.256	175	160.3	0.16	175	0.10%
4	500	0.513	175	160.3	0.321	175	0.20%
5	500	1.282	175	160.3	0.801	175	0.50%
6	500	2.564	175	160.3	1.603	175	1.00%

7	500	3.846	175	160.3	2.404	175	1.50%
---	-----	-------	-----	-------	-------	-----	-------

80

81 Cement pastes with raw and sonicated CNCs are studied in this work. 30 minutes of sonication was
82 performed to disperse the CNCs in the aqueous suspension. This sonication technique and the
83 experimental details can be found in the previous paper [4].

84

85 **2.3. Centrifugation**

86 A centrifugation method is established to quantify the concentrations of the aCNC and fCNC. At the age
87 of 15 min (from the time of mixing), approximately 250 g fresh cement pastes are transferred into a
88 Sorvall RC-3C Plus high capacity centrifuge. The centrifugation was performed at 5000 rpm for 20 min
89 and the liquid on top of the cement was collected. The collected liquid was then filtered three times with
90 filter paper to remove the cement particles. Previous control tests on the CNC aqueous suspensions
91 showed that most of the CNCs (>99.5%) passed through the filter paper, and therefore the loss of CNCs
92 due to filtration was not accounted for. The filtered liquid was then weighed and dried in an oven at 50 °C
93 for 48 hours. For the plain cement paste, the final products after oven-drying are the salts and alkalis in
94 the pore solutions [6], while for the cement paste with CNCs, the solids also contain the fCNCs. By
95 comparing the solids concentrations obtained from the two different cement pastes, the concentrations for
96 the fCNCs as well as the aCNCs can be calculated.

97

98 **2.4. Isothermal Calorimetry**

99 Isothermal calorimetry tests were performed to study how the sonication influences the hydration process
100 of the cement pastes. A TAM Air isothermal calorimeter was used with a temperature of 23 ± 0.1 °C [7].
101 After the cement paste mixing, approximately 30 g of the sample was immediately transferred to a glass
102 ampoule (22 mm in diameter and 55 mm in height), which was then sealed and placed into the
103 calorimeter for measurement. Before the data collection started, the isothermal condition was held for 45
104 min to reach equilibration and the subsequent steady heat measurement was performed for approximately
105 200 hours.

106

107 **2.5. Nanoindentation**

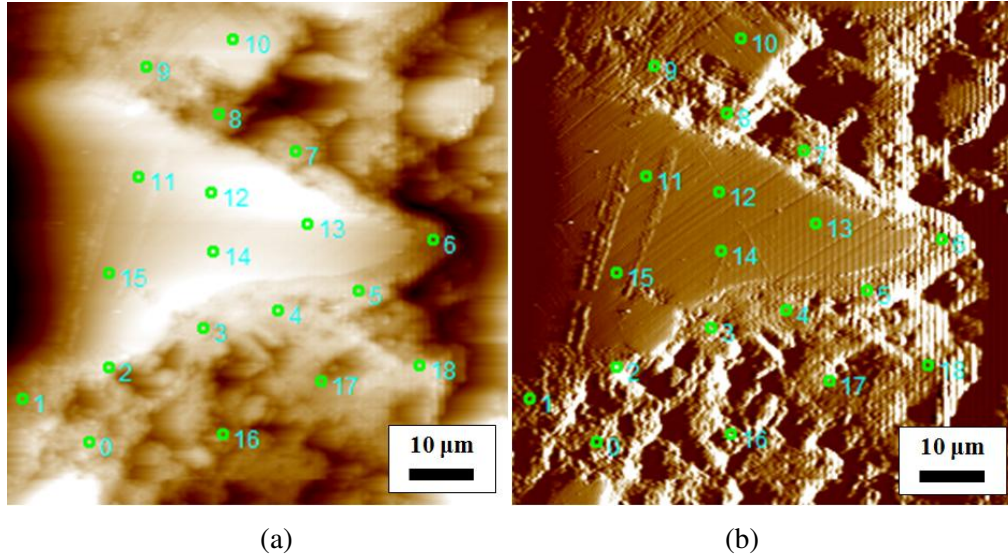
108 One link between the CNC distribution in the cement paste and the mechanical performance at the macro-
109 level, e.g., the flexural strength, is the CNCs influence on the microstructural mechanical properties. To
110 investigate the local variations of the material behavior within cement microstructures nanoindentation
111 has been used in the areas of interfacial transition zone in concrete [8] to study the micro-mechanisms of
112 creep in CSH phases [9], and conduct statistical analysis of the nano-mechanical properties governing the

113 ultra-high performance concrete microstructure [10]. As CNCs have completely different materials
114 properties from cement, they may alter the microstructural properties of cement paste, e.g. elastic
115 modulus and hardness, and these changes may vary significantly with higher concentration of CNCs. For
116 this reason, the microstructural properties may be indicative of the CNCs distribution in the cement pastes.
117 Since CNCs are prone to adsorb on cement surface, a high concentration is expected to be found in the
118 high density CSH region for a hardened cement paste. In this work, nanoindentation was performed at
119 three different phases in the hardened cement pastes: the unhydrated cement particle, high density CSH
120 and low density CSH to study how the mechanical properties were influenced by CNCs. The mechanical
121 properties obtained from nanoindentation were the reduced indentation modulus E_r and hardness H .

122

123 Three different cement pastes samples were prepared for the nanoindentation: plain (reference), one with
124 1.5 vol. % raw CNCs and one with 1.5 vol. % sonicated CNCs, all of which were sealed at 23 °C after
125 cast. At the age of 28 days they were demolded and cut with a low-speed oil saw to expose a fresh surface.
126 A lapping procedure at 45, 30, 15 μm with paraffin oil for 12 min each and a polishing procedure using 9,
127 6, 3, 1, 0.25 μm diamond paste for 20 min each on top of Texmet paper were conducted on the sample
128 surface. These procedures are similar with the methods described elsewhere [11, 12]. The nanoindentation
129 tests were performed on the three different phases: the unhydrated cement particles, the high density CSH
130 and the low density CSH with a TI 950 TriboIndenter [13] from Hysitron Corporation. For each test,
131 multiple indents (greater than 5) were measured for each phase, and post indentation evaluation
132 confirmed the location of each indent was in the desired phase. Figure 2 shows a scanning probe
133 microscopic (SPM) image obtained with the indenter at the scanning mode on a $50\mu\text{m}\times 50\mu\text{m}$ sample
134 surface: Fig. 2 (a) is the topographic image and (b) the gradient image. The triangular shaped particle in
135 the middle of the figures is the unhydrated cement particle and the features in the relatively uneven area
136 surrounding the particle are the hydration products. The dots with numbers show the locations where
137 indentation was performed. In this case, locations 1-9 correspond to interfacial region, 10-15 to the
138 unhydrated cement particle and 16-18 to the matrix (low density CSH). The distance between
139 nanoindentations was maintained to be greater than $\sim 10\ \mu\text{m}$ in all these cases.

140



141
142
143
144
145

Fig. 2. The locations picked for the nanoindentation on the (a) topographic image; (b) gradient image on a 50 μm × 50 μm area

146 For all nanoindentation experiments, a single load function was applied with 4000 μN in load-controlled
147 mode. The loading rate is 800 μN/sec. Subsequently the load is kept constant for 5s in order to minimize
148 creep behavior within various phases of the paste matrix. Otherwise, the viscoelastic and creep properties
149 can result in significant bowing in the unloading curves, which might affect the data analysis of
150 nanoindentation. Unloading rate is 800 μN/sec. In this given indentation experiment, the peak load (P_{max}),
151 the contact depth at the peak load (h), and the slope of the unloading curve ($S = dP/dh$) were obtained.
152 The reduced indentation modulus E_r was determined following [14]:

$$E_r = \frac{dP}{dh} \frac{\sqrt{\pi}}{2\sqrt{A}} \quad \text{(Equation 1)}$$

153
154
155
156
157
158

where A is the projected contact area, which needs to be calculated from the indenter geometry (Berkovich) and contact depth (h) based on previous calibration on the reference materials. dP/dh is the slope of unloading curve in the load-depth curve.

159 2.6. Scanning Electron Microscopy (SEM) and Energy-Dispersive X-ray (EDX) Spectroscopy

160 The EDX technique has been widely employed for the elemental analysis on the chemical compositions
161 of cement composites [15-17]. In this work EDX was performed to investigate the CNC distribution in
162 the hardened cement pastes with an FEI Quanta 3D FEG equipment. Three specimens were studied: the
163 plain cement paste (reference), one with 1.5 vol. % raw CNCs and one with 1.5 vol. % sonicated CNCs.
164 Ideally the element carbon should help to locate the CNCs in the cement pastes since cement does not

165 contain carbon while CNCs ((C₆H₁₀O₅)_n) do. However, based on the preliminary EDX results, carbon was
 166 detected over the entire surface of the cement paste specimen, which was likely due to the carbonation [18,
 167 19], even when all the specimens were carefully stored in a desiccator. For this reason this work focuses
 168 on the oxygen spectroscopy and studies how the oxygen concentration fluctuates at different phases in the
 169 cement paste. As the condition for the imaging and EDX signal acquisition might be different for
 170 different specimens, the signal intensities cannot be directly compared with each other, and therefore a
 171 normalization was performed for the oxygen spectroscopy with the signals collected from the unhydrated
 172 cement cores as a base. Since the CNCs cannot penetrate into those cores, the chemical compositions as
 173 well as the oxygen concentration should be always the same at the core. With a normalization based on
 174 the oxygen concentration within the cores, the signals can be compared between EDX results for different
 175 specimens without taking into account of the experimental conditions. The normalization of the signal
 176 counts was done with following procedures: The oxygen signals collected within the unhydrated cement
 177 cores were picked and the average count (intensity) in this region was calculated as N_{ave} , and then all the
 178 original oxygen signal intensity I_{ori} in the same mapping were divided by N_{ave} to obtain the normalized
 179 intensity I_{nor} , as shown in following equation:

$$I_{nor} = \frac{I_{ori}}{N_{ave}} \quad \text{(Equation 2)}$$

181

182 **2.7. Water desorption**

183 The equilibrium relative humidity (RH_{eq}) at which the transition happens between condensation and
 184 evaporation of the liquid inside a pore can be related with the pore radius and the liquid properties with
 185 the well-known Kelvin equation [20, 21]:

$$\ln(RH_{eq}(r)) = \frac{rRT}{2\gamma V_m} \quad \text{(Equation 3)}$$

187

188 where γ is the surface tension, V_m the molar volume of the fluid, R the universal gas constant, r the radius
 189 of the pore, T the temperature. The water desorption with a decreasing RH for the water saturated
 190 hardened cement paste was measured with a Q5000 SA absorption/desorption analyzer from TA
 191 instruments. Three different specimens were studied: plain cement paste, a cement paste with 1.5 vol. %
 192 raw CNCs and a cement paste with 1.5 vol. % sonicated CNCs. The cement pastes were demolded at the
 193 age of 28 days and a 1-mm thick specimen was obtained with a low-speed oil saw. The specimens were
 194 vacuum saturated by placing them in a desiccator and evacuating the air for 8 hours, and then back-filled
 195 with vacuum de-gassed for another 3 hours. After taken out from the vacuumed water, the surface
 196 moisture of the fully saturated specimens were wiped with a Kimwipes delicate task wiper mildly and
 197 quickly (within ~3 seconds) and then the specimens were immediately transferred to the equipment to

198 avoid the evaporation of the water from pores. The initial RH in the chamber was 97.5%, and then the RH
 199 was decreased with 10% steps, and a final step of 17.5% to reach 0%.

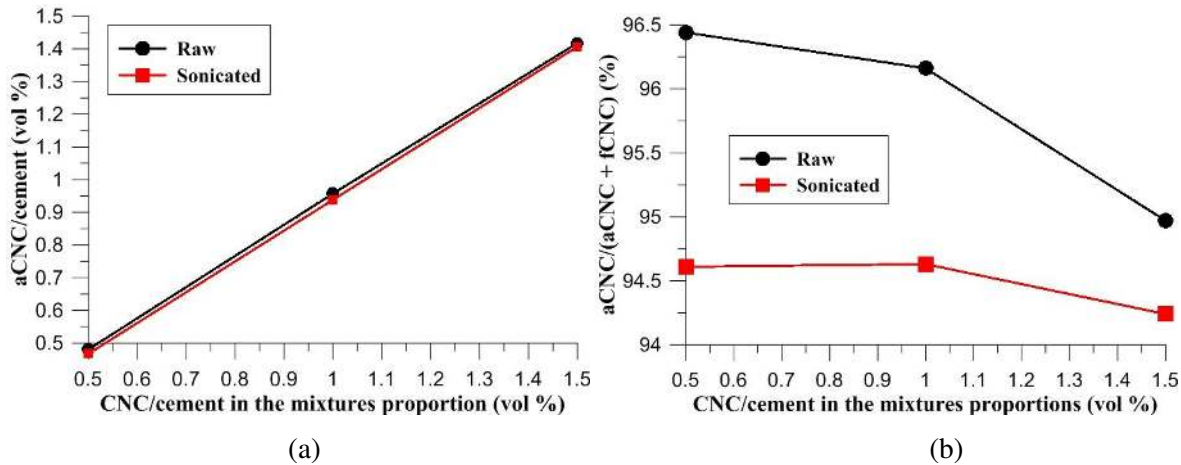
200

201 **3. Results and discussions**

202 **3.1. The concentration of aCNCs and fCNCs**

203 The amount of aCNCs and fCNCs adhered on the cement particles was quantified by the centrifugation
 204 method described in Section 1.3. We analyzed three different concentrations: 0.5 vol. %, 1.0 vol. % and
 205 1.5 vol. % with and without sonication (raw) (Mixtures #5, 6 and 7 in Table 2). Figure 3 (a) shows the
 206 mass of the aCNCs per gram of cement and (b) gives the aCNC percentages out of all CNCs, i.e.,
 207 aCNCs/(fCNC+ aCNCs) %. The results in Fig. 3 (a) indicate that, with increasing the CNC concentration
 208 (from 0.5 vol. % to 1.5 vol. %) the aCNC/cement percentage increases almost linearly and is not affected
 209 by sonication. This means that the CNCs keep adsorbing on the cement surface. Figure 3 (b) shows that
 210 the percentage of the aCNCs out of all CNCs does not change much, and is not necessarily affected by
 211 sonication (within measurement uncertainty). In conclusion, the majority of the CNCs (94.2% to 96.5%)
 212 are adsorbed on the cement surface, regardless of the total amount of CNCs added in the cement paste.
 213 This result suggests that, while sonication disperses CNC agglomerates [4], it does not exchange aCNCs
 214 for fCNCs.

215



216

217

218 Fig. 3. (a) The mass of the aCNCs per gram of cement and (b) the aCNC percentages out of all CNCs

219

220 A simple calculation is given here to estimate the maximum surface area of cement particles that can be
 221 covered by CNCs with an assumption that all the CNCs lie on the surface with one of their sides and there
 222 is no overlapping of CNCs. Assume the total mass of all CNCs is m , and the total volume as $m/\text{density}$,
 223 then the total length of all CNCs is $L = (m/\text{density})/(\text{CNC cross-section})$. Given that the cross-section of
 224 the CNC is approximately $4 \times 4 \text{ nm}^2$ square (the width can range from 3~5 nm according to [1]), the

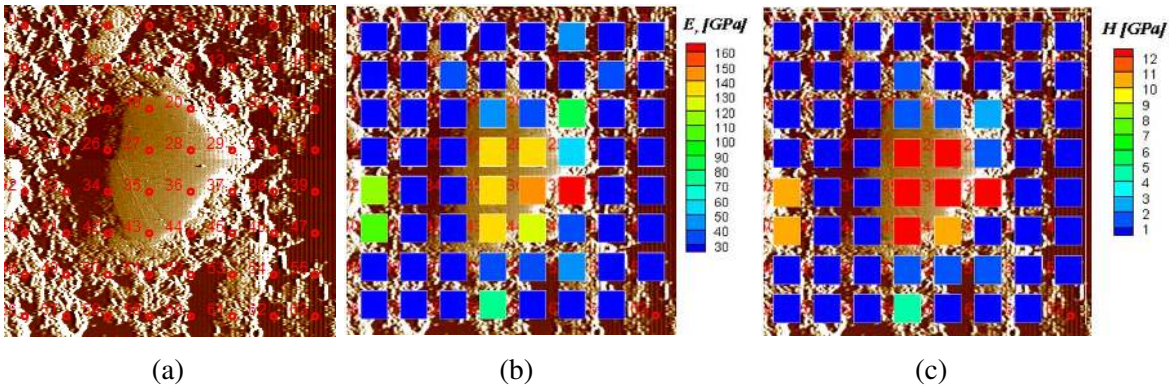
225 maximum area covered with CNCs is then $A = L \times 4 \text{ nm}$. For every kg of cement, at the CNC/cement vol
 226 concentrations of 0.5%, 1.0% and 1.5%, the maximum surface coverage by CNCs (m^2/kg) is calculated as
 227 400, 800, and 1200 m^2 , respectively. As the Blaine fineness (surface area per unit kg cement) of the
 228 cement used in this work is $316 \text{ m}^2/\text{kg}$, CNCs can cover all the surface of cement for the three
 229 concentrations in this ideal situation. However, this calculation does not account for the fCNCs, and more
 230 important, the overlapping of the aCNCs on the cement surface, which is highly possible given the
 231 agglomeration of CNCs in the fresh cement paste [2]. For these reasons, the actual area covered by CNCs
 232 should be smaller than the values calculated above, and is also smaller than the total surface area of
 233 cement, given that the adsorption continues to occur without reaching any limit (Fig. 3 (a)).

234

235 **3.2. Nanoindentation**

236 Nanoindentation was performed to study the CNCs distribution in the cement pastes at an age of 28 days
 237 and their influence on the local mechanical properties. Three different specimens were analyzed: the plain
 238 cement paste, one with 1.5 vol. % raw CNCs and one with 1.5 vol. % sonicated CNCs. A representative
 239 mapping of the reduced modulus and hardness is shown in Fig. 4. As expected, the unhydrated cement
 240 particle shows much higher reduced modulus and hardness than the matrix phase [22].

241



242

243

244 Fig. 4. (a) An area containing an unhydrated cement particle and matrix for the plain cement paste; the
 245 mapping of (b) reduced modulus and (c) hardness on this area

246

247 As stated earlier, the interfacial region between the unhydrated cement and the matrix is likely to contain
 248 the highest concentration of CNCs, and therefore is the phase of main interest. The reduced modulus is
 249 plotted as a function of the contact depth as shown in Fig. 5(a) for all the three different phases, from
 250 which it can be observed that for the three different specimens, the reduced moduli are close at the cement
 251 particle and matrix phase. This can be more clearly observed in Fig. 5(b), which shows the data obtained
 252 only from the low density CSH and the unhydrated cement. Finally, Fig. 5(c) shows the reduced modulus

253 for the interfacial regions. In the plots the data on the interfacial region are designated as the solid
 254 symbols and the data from the other two phases (unhydrated cement and matrix) are open symbols. The
 255 data in Fig. 5(c) are fit with a power law and the two specimens with CNCs show trendlines which are
 256 higher than the reference. The fitting equations are given as:

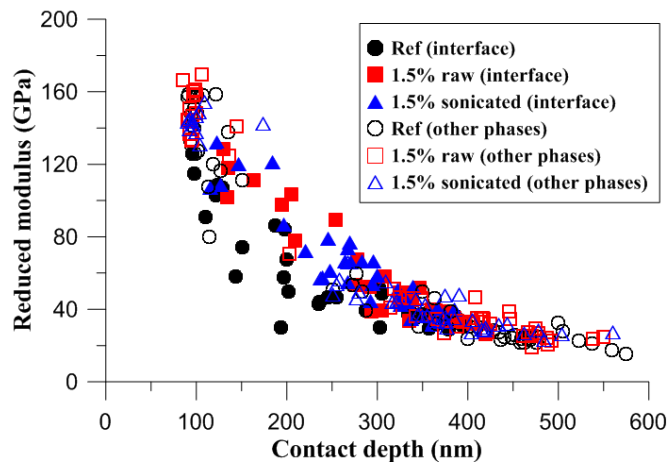
257 Ref: $y = 7119x^{-0.91}$ (Equation 4)

258 1.5% raw: $y = 49714x^{-1.21}$ (Equation 5)

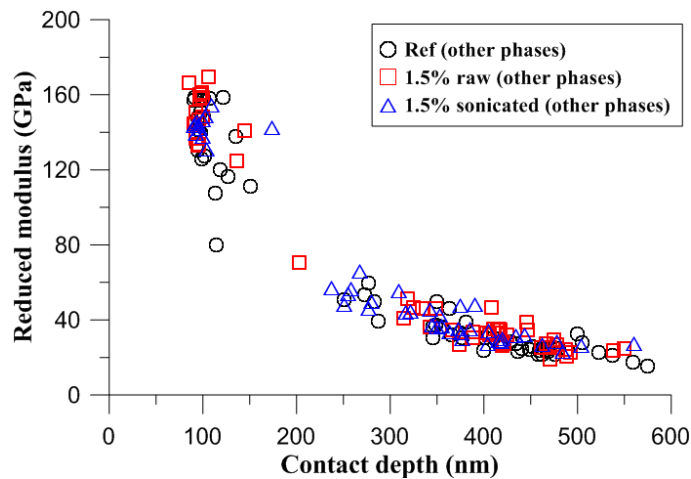
259 1.5% sonicated: $y = 19309x^{-1.03}$ (Equation 6)

260
 261 The reduced modulus results indicate that the unhydrated cement and low density CSH are not affected
 262 much by CNCs, which is expected since most CNCs are in the high density CSH. Moreover on the high
 263 density CSH, the reduced modulus is improved with raw and sonicated CNCs.

264
 265



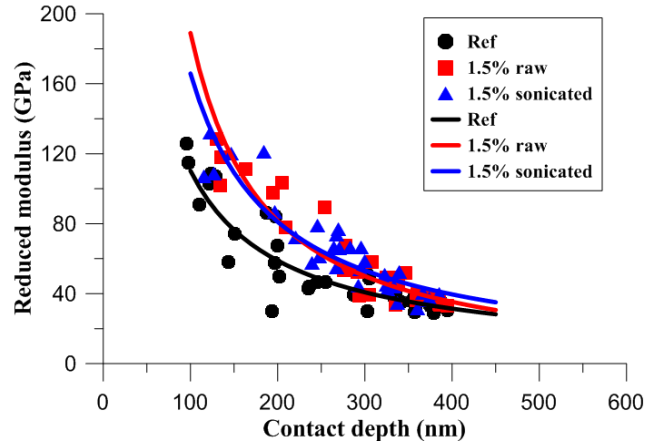
(a)



(b)

266
 267

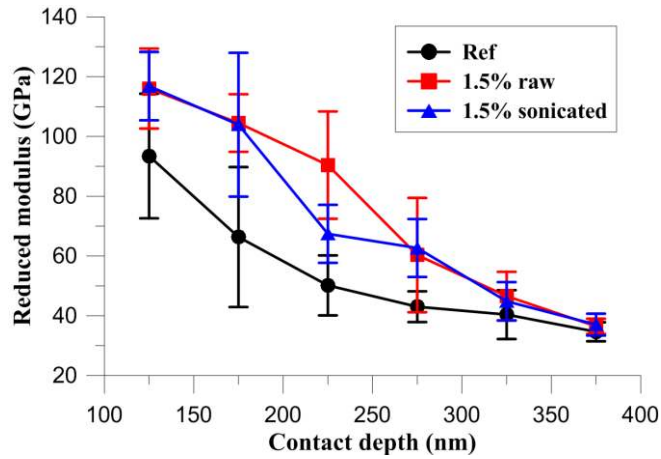
268
 269



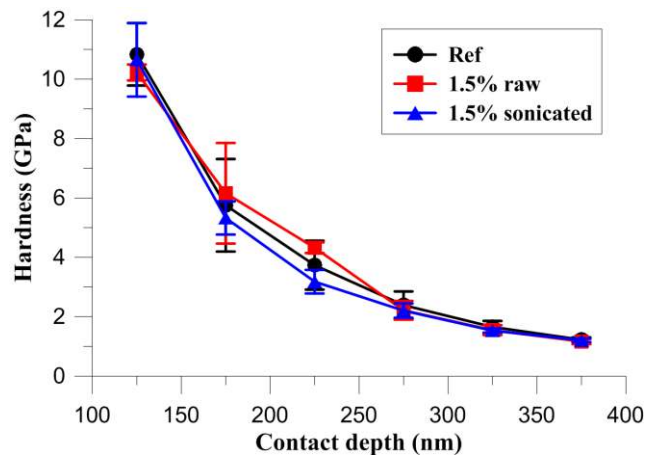
(c)

Fig. 5. The relationship between the reduced modulus and contact depth (a) at all three different phases; (b) at the unhydrated cement and low density CSH; (c) at the interfacial regions

The reduced modulus and the hardness for the interfacial regions are grouped based on the contact depth with a bin size of 50 nm to obtain average values. For example, the reduced moduli within the contact depth between 100 ~ 150 nm are grouped to calculate the average reduced modulus, which is then reported by the average contact depth 125 nm in Fig 6. Figure 6 (a) shows that with CNC additions, the reduced modulus is increased significantly compared with the plain cement paste (reference), especially below the contact depth of 300 nm. For example, the average reduced modulus for the contact depth 150~200 nm was increased from ~70 GPa to ~105 GPa with CNC additions, which is 50% improvement. The reason for the improvements may be the high elastic modulus of CNCs, which ranges from 110 to 220 GPa [1, 23, 24], which is higher than that of the interfacial region (high density CSH) with the value about 40~110 GPa. If it is assumed that the mechanical properties of the “composites” constituted by the high density CSH and the CNCs follow a mixtures law, the modulus of high density CSH can be increased by CNCs. Another possible reason is that CNC additions caused a modification to the CSH (e.g. its structure, or chemistry, etc) which may also have altered the modulus. Figure 6 (b) shows that with CNC additions, the hardness does not change much in the interfacial regions, the maximum change with respect to the reference is ~10%, which is much smaller than the influence in the reduced modulus.



(a)



(b)

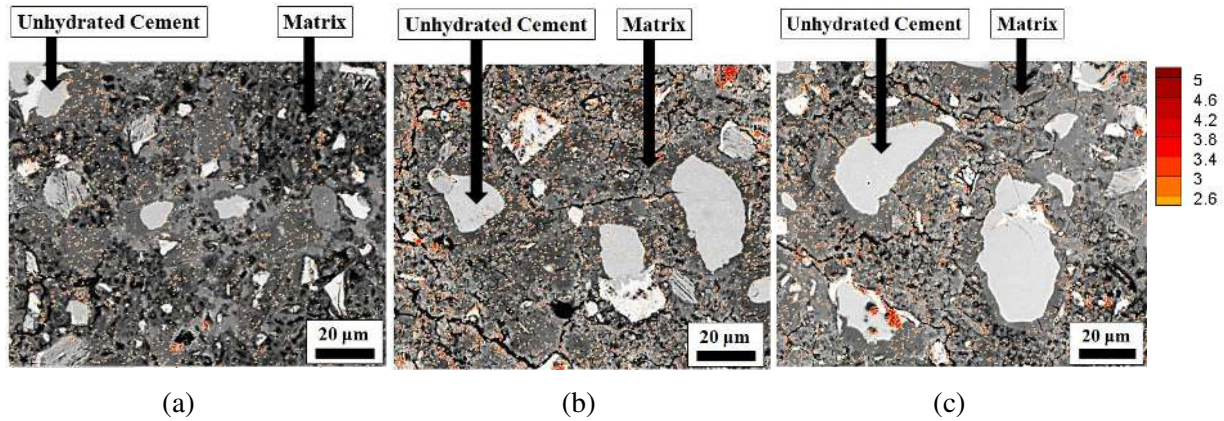
Fig. 6. (a) The average reduced modulus and (b) the average hardness on the interfacial regions

3.3. EDX and SEM

The results of the oxygen mapping for the three specimens are shown in Fig. 7 overlapping the original SEM images and the mappings without SEM images are provided in Fig. 8. In the mapping, the signals with intensity below 2.6 (this chosen value is approximately the smallest number that the oxygen signals inside the unhydrated cement can be removed) are truncated and only the signals above that are shown (higher intensity means higher oxygen concentration). From Fig. 8 (a) it can be observed that only very few oxygen signals are observed inside the unhydrated cement cores compared with the matrix phase. This difference is due to the oxygen from chemically bound water in the hydration products. By comparing the mappings between the reference and the two specimens with CNCs (Figs. 8b and c), it is found that the oxygen concentration is much higher in the matrix phase and the interfacial region, which indicates the distribution of CNCs. Based on the visualization, however, it is difficult to observe a significant difference between the specimens with raw and sonicated CNCs. Oxygen spectroscopy is

309 performed along a scanning-line (red) across one or more unhydrated cement particles to make a
 310 quantitative comparison between the three specimens, as shown in Fig. 9. For the plain cement paste
 311 (reference), the spectroscopy is relatively stable that most of the peaks are below the intensity of 3, while
 312 the two specimens with CNCs, there are a few high peaks which are highlighted with dashed lines
 313 denoting their corresponding locations in the cement pastes (the intensity of 3 is plotted with the thin
 314 black line in Fig. 9). It is noteworthy that the locations of the peaks are different for the specimens with
 315 raw and sonicated CNCs. For the one with raw CNCs, most of the peaks are found at the interfacial
 316 region between cement particle and the matrix, while for the one with sonicated CNCs, the peaks are
 317 randomly distributed along the scanning line. This result indicates that, without sonication, a high
 318 concentration of CNCs are prone to stay at the interfacial region, while after sonication they are more
 319 randomly dispersed into the matrix phase.

320



321

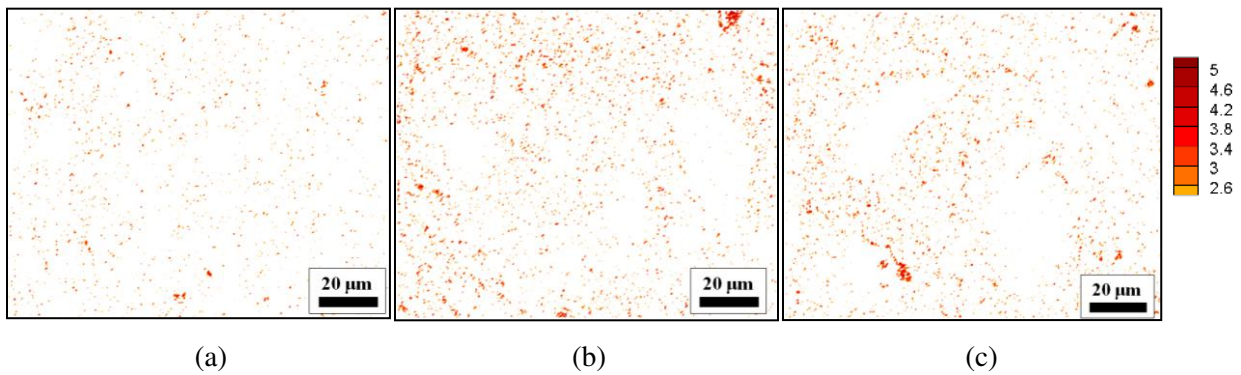
322

323

324

325

Fig. 7. Oxygen mapping with SEM images of (a) plain cement paste; (b) with 1.5 vol. % raw CNCs and (c) with 1.5 vol. % sonicated CNCs



326

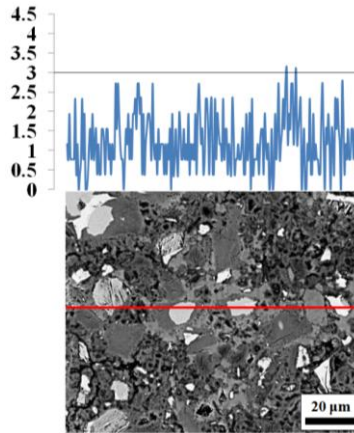
327

328

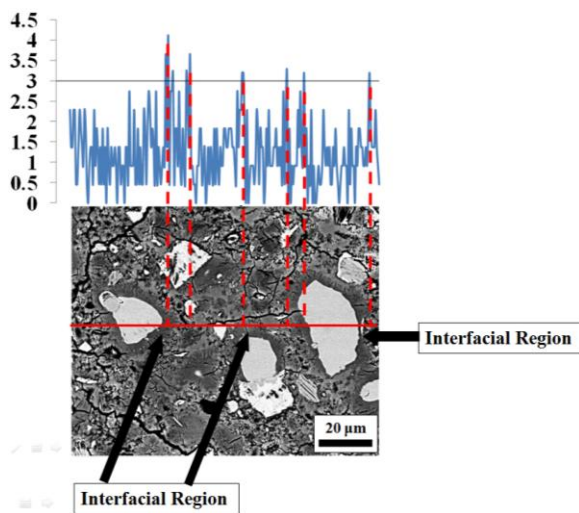
329

330

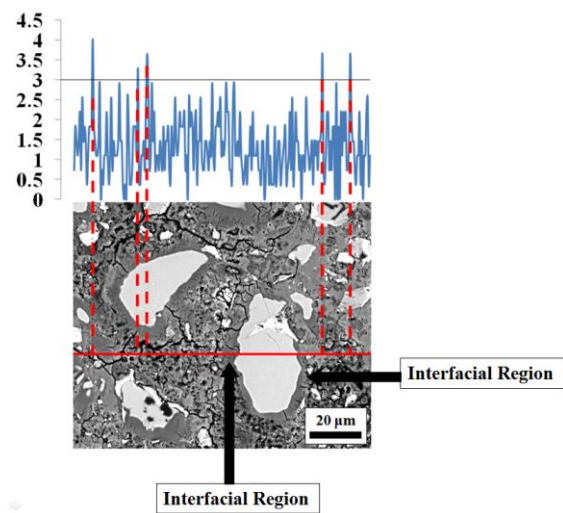
Fig. 8. Oxygen mapping alone of (a) plain cement paste; (b) with 1.5 vol. % raw CNCs and (c) with 1.5 vol. % sonicated CNCs



(a)



(b)



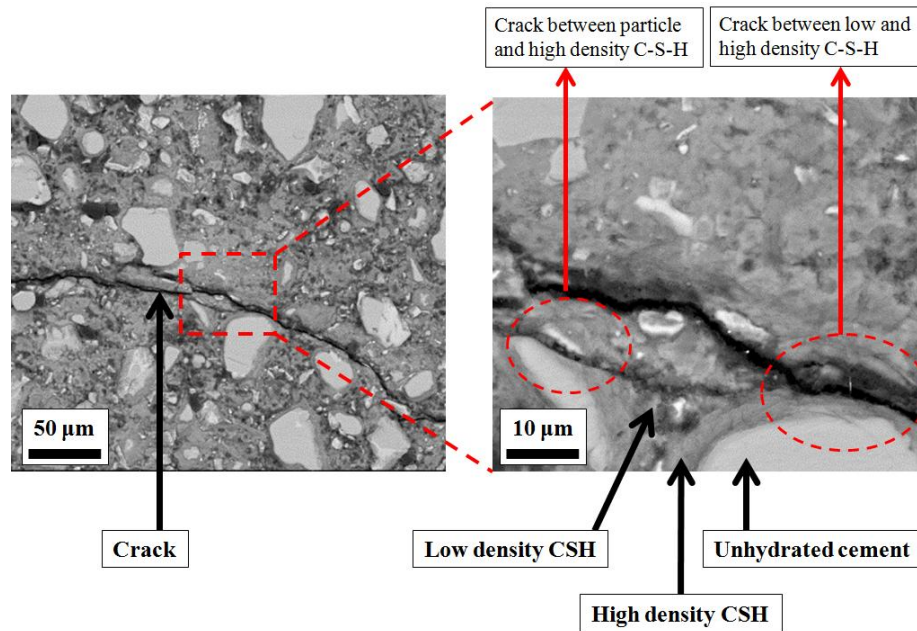
(c)

Fig. 9. Line-scanning spectroscopy of oxygen of (a) plain cement paste; (b) with 1.5 vol. % raw CNCs and (c) with 1.5 vol. % sonicated CNCs

As previously discussed, most of the CNCs are adsorbed on the cement surface in the fresh cement paste regardless of whether sonication was employed. However the CNCs cannot be distinctly classified as the aCNCs or fCNCs in the hardened cement paste. In fact, CNCs are found distributed in the matrix phase, both high and low density CSH. This fact means that, during the CSH growth, some of CNCs are embedded in the high density CSH while some others move away from the cement particles into the low density region.

Multiple cracks are observed from the SEM images. Fig. 10 shows an example of the cement paste with raw CNCs. It can be observed that, the cracks pass through two different paths: one between the unhydrated cement particle and the high density CSH, and the other between low (matrix phase) and high

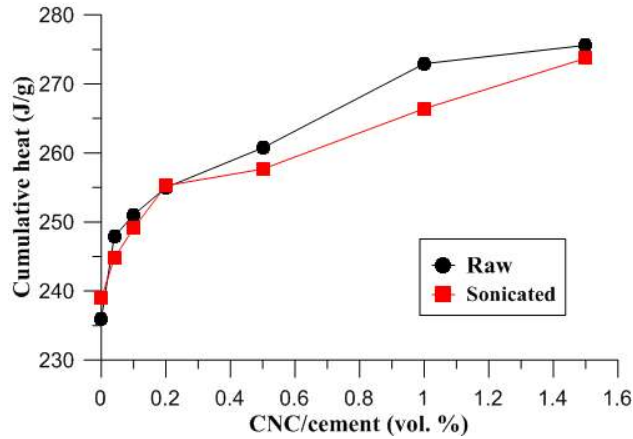
348 density CSH, as circled in Fig. 10. The SEM images here may indicate that the crack can randomly pass
349 through different interfaces regardless of CNC concentrations.
350



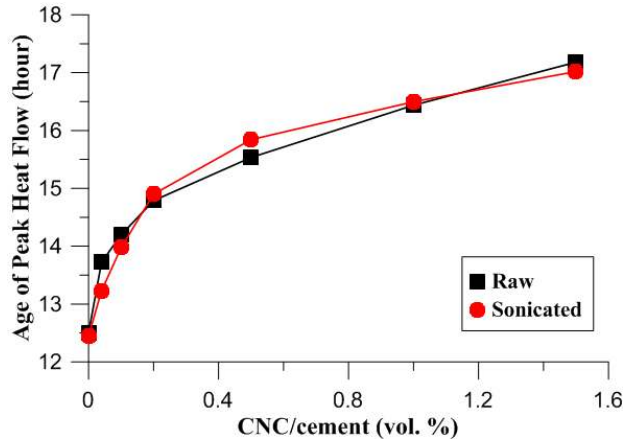
351
352 Fig. 10. SEM images show multiple cracks in the cement paste with 1.5 vol. % raw CNCs
353

354 3.4. Isothermal calorimetry

355 The cumulative heat release at the age of 168 hours are summarized in Fig. 11 and the values are
356 generally very similar for different concentrations. Figure 12 summarizes the relationship between the
357 ages of the heat flow peak with the CNC concentration for the two different CNCs, which shows that the
358 delay in hydration is not influenced much by sonication. As a summary, the cement pastes with raw and
359 sonicated CNCs do not show significant differences in the cumulative heats at the age of 7 days (168
360 hours) or the hydration processes. This seems to indicate that although the CNCs are more dispersed with
361 sonication, the effect of SCD as a whole is not affected significantly. This result is not unexpected since it
362 was found that after sonication, the concentration of aCNCs did not appear to change much.
363



364
 365 Fig. 11. Cumulative heats comparison between the cement pastes with raw and sonicated CNCs at the age
 366 of 168 hours
 367



368
 369 Fig. 12. The ages of the peak flow of the cement pastes with raw and sonicated CNCs
 370

371 In the previous paper [2], it was established that steric stabilization is one of the mechanisms that CNCs
 372 use to improve the DOH, which is similar with what the polycarboxylate-based water-reducing agent
 373 (WRA) does in the cement paste. A parallel hydration study was performed on the cement pastes with
 374 varying dosages of a polycarboxylate-based WRA (ADVA 140). As expected, with WRA, the dormant
 375 period is significantly extended as shown in Fig. 13 that, the heat flow peak delay for the 1.5 vol. % WRA
 376 cement paste is about 15 hours, which is much longer than that of the 1.5 vol. % CNC cement paste (~ 4.5
 377 hours). This is because the hydrophobic chains [25] of the WRA block water from reaching the cement
 378 surface, while the hydrophilic and hygroscopic nature of CNCs [3] lead to SCD, although both WRA and
 379 CNCs can be adsorbed on the cement surface.

380

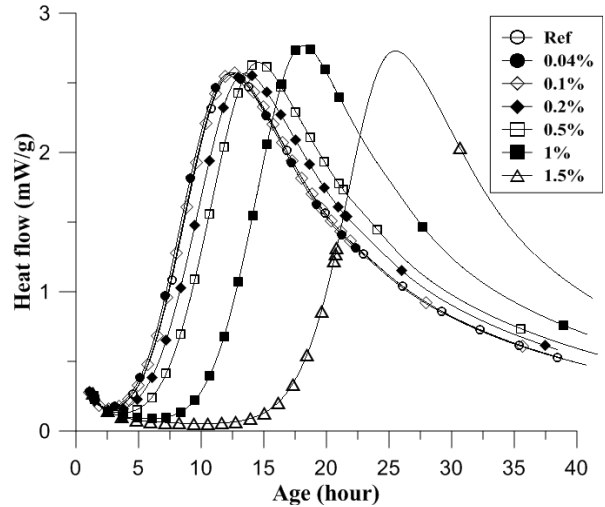


Fig. 13. Heat flow curves of cement pastes with WRA

381
382
383
384
385
386
387
388
389
390
391
392

3.5. Pore size distribution

Water desorption tests were performed to study the CNCs influence on the pore size distribution of the cement pastes. Mindness et al. [26] classified pores with respect to the pore radius: small capillary pores (cap.) of 1.25 nm to 5 nm, medium capillary pores 5~25 nm, large capillary pores >25 nm and gel pores with the radius below 5 nm. In the work by Villani et al. [20], they provided a plot of the relationship between the pore radius and the RH_{eq} of water based on the Kelvin Equation. Figure 14 summarizes the pore size ranges of different types of pores and the RH_{eq} values corresponding to the boundaries of different pores.

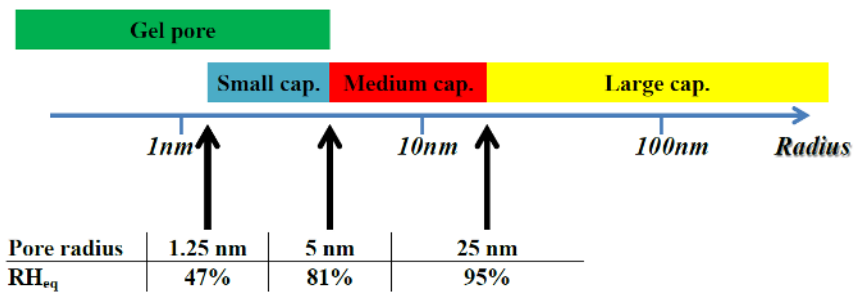


Fig. 14. The size ranges of different pores and the corresponding RH_{eq}

393
394
395
396
397
398
399
400

The water content as a function of RH_{eq} is shown in Fig. 15 for the three specimens. The two specimens with CNCs show a reduction in the water content compared with the plain cement paste. This result is expected, as CNCs can improve the DOH of cement paste, and a consequent result is the reduction of the total porosity.

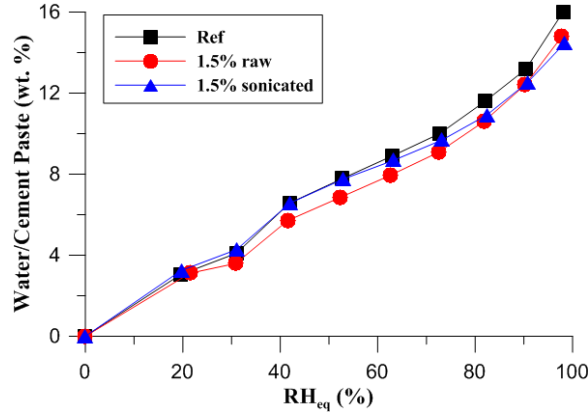
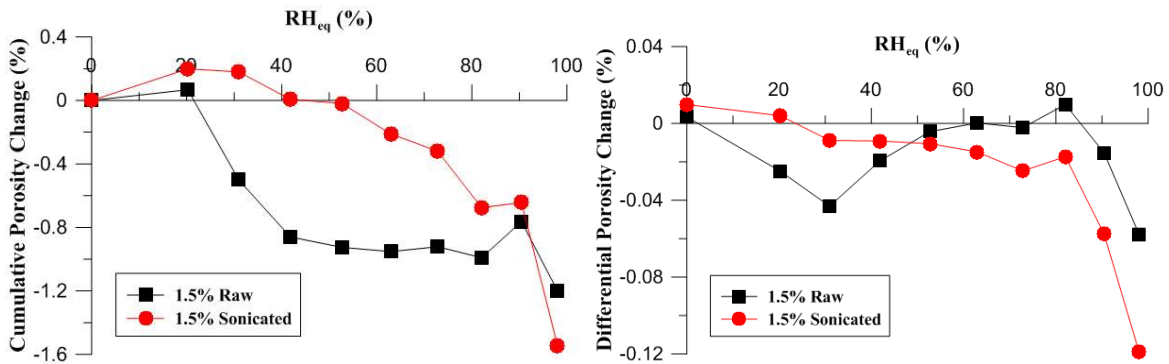


Fig. 15. The relationship between the water content and the RH_{eq}

401
 402
 403
 404
 405
 406
 407
 408
 409
 410
 411
 412
 413
 414
 415
 416
 417
 418
 419

The porosity differences (in percentage) between the specimens with CNCs and plain cement paste (reference) at different RH_{eq} are plotted versus the RH_{eq} in both cumulative and differential values are shown in Fig. 16. The total porosity reductions (at the RH_{eq} = 97.5%) for the cement pastes with raw and sonicated CNCs are 1.2% and 1.6%, respectively. Without sonication, the CNC agglomerates adsorb water and the unreacted water may form the capillary pores. In addition, the CNC agglomerates may bring air entrapment which also increases porosity. As a result, the porosity reduction with sonicated CNCs is larger than that with raw CNCs. For high values of RH_{eq} (> 50%), the sonicated CNCs reduce the porosity when compared to the raw ones because there are fewer CNC agglomerates and the dispersed single CNCs cannot cause either high concentration of water around them or air entrapment. However, at the low RH_{eq} region (< 50%), the raw CNCs lead to more pore reduction than the sonicated CNCs. Within this RH_{eq} range, the pores are classified as the small gel pores (Fig. 14), which are included in the space occupied by the hydration products [26]. The results in Fig. 16 may indicate that the dispersed single CNCs lead to a certain amount of gel pores around them. In summary, CNC agglomerates attract a large amount of water, which lead to capillary pores, while single CNCs attract a small amount of water, which lead to gel pores.

420



421 (a) (b)
422 Fig. 16. (a) The cumulative porosity change and (b) the differential porosity change of the cement pastes
423 with raw and sonicated CNCs from the reference
424

425 **3.6. Discussion**

426 The centrifugation experiment indicates that after sonication, the majority of the CNCs are still the
427 aCNCs. It is observed from the calorimetry results that the hydration process is not influenced much with
428 sonication, which is consistent with the centrifugation result. Given that the CNC agglomerates are
429 reduced with sonication, it appears that the aCNCs are more uniformly distributed on cement surface after
430 sonication. EDX results verifies this hypothesis that for raw CNCs, the oxygen is more concentrated on
431 the high density CSH, while with sonication, CNCs are more dispersed. The pore size distribution study
432 shows that sonication helps reduce the porosity at the large size range, i.e., the capillary pores, which is
433 also a result of the reduction in agglomerates. The nanoindentation results also indicate that there are high
434 concentrations of CNCs in the high density CSH and the reduced modulus at the high density CSH is
435 increased with CNC additions.

436

437 **4. Conclusions**

438 This paper studies how sonication influences the CNCs distribution in both fresh and hardened cement
439 pastes and how it modifies the microstructures of the pastes. Although sonication can disperse the CNC
440 agglomerates, the dispersed CNCs remain adsorbed on cement surface in the fresh cement paste. For the
441 hardened cement paste, it is found that sonication helps reduce the large size porosity. The
442 nanoindentation results show that the reduced modulus at the high density CSH is increased with CNC
443 additions, possibly due to the high modulus of the CNCs.

444

445 **Acknowledgements**

446 This work was supported by the National Science Foundation through Awards no. CMMI #1131596. The
447 authors are grateful for the USFS Forest Products Laboratory for providing the CNC materials.

448

449 **References**

- 450 [1] Moon RJ, Martini A, Nairn J, Simonsen J, Youngblood J. Cellulose nanomaterials review: structure,
451 properties and nanocomposites. *Chem Soc Rev.* 2011;40(7):3941-94.
452 [2] Cao Y, Zavattieri PD, Youngblood J, Moon RJ, Weiss J. The influence of cellulose nanocrystal additions
453 on the performance of cement paste. *Cem Concr Compos.* 2015;56:73-83.
454 [3] Taib RM. Cellulose fiber-reinforced thermoplastic composites: processing and product characteristics.
455 Blacksburg, Virginia, Virginia Polytechnic Institute and State University; 1998.

456 [4] Cao Y, Zavattieri PD, Youngblood J, Moon RJ, Weiss J. The relationship between the dispersion of
457 cellulose nanocrystals and strength improvements. in preparation for Construction and Building
458 Materials.

459 [5] Laboratory FP. Nanocellulose Pilot Plant. <http://www.fpl.fs.fed.us/>; Forest Products Laboratory; 2009.

460 [6] Rajabipour F, Sant G, Weiss J. Interactions between shrinkage reducing admixtures (SRA) and cement
461 paste's pore solution. *Cem Concr Res.* 2008;38(5):606-15.

462 [7] TA-Instruments. TAM Air Isothermal Calorimetry.
463 <http://www.tainstruments.com/main.aspx?siteid=11&id=217&n=4>; TA-Instruments; 2013.

464 [8] Li W, Xiao J, Sun Z, Kawashima S, Shah S. Interfacial transition zones in recycled aggregate concrete
465 with different mixing approaches. *Constr Build Mater.* 2012;35:1045-55.

466 [9] Acker P. Micromechanical analysis of creep and shrinkage mechanisms. In: Ulm F, Bažant Z, Wittman
467 F, editors. *Creep, Shrinkage and Durability Mechanics of Concrete and other Quasi-Brittle Materials.*
468 Oxford, UK: Elsevier; 2001.

469 [10] Sorelli L, Constantinides G, Ulm F, Toutlemonde F. The nano-mechanical signature of ultra high
470 performance concrete by statistical nanoindentation techniques. *Cem Concr Res.* 2008;38(12):1447-56.

471 [11] Ashraf W, Olek J, Tian N. Nanomechanical Characterization of the Carbonated Wollastonite System.
472 Fifth International Symposium on Nanotechnology in Construction 2015. p. 7.

473 [12] Hughes JJ, Trtik P. Micro-mechanical properties of cement paste measured by depth-sensing
474 nanoindentation: a preliminary correlation of physical properties with phase type John J. Hughesa, , ,
475 Pavel Trtikb, . *Mater Charact.* 2004;53(2-4):9.

476 [13] Hysitron. <http://www.hysitron.com/products/ti-series/ti-950-triboindenter>.

477 [14] Oliver W, Pharr G. An improved technique for determining hardness and elastic modulus using load
478 and displacement sensing indentation experiments. *J Mater Res.* 1992;7(6):20.

479 [15] Famy C, Brough A, Taylor H. The C-S-H gel of portland cement mortars: part I. the interpretation of
480 energy-dispersive X-ray microanalyses from scanning electron microscopy, with some observations on C-
481 S-H, AFm and AFt phase compositions. *Cem Concr Res.* 2003;33:1389-98.

482 [16] Diamond S. Identification of hydrated cement constituents using a scanning electron microscope -
483 energy dispersive X-ray spectrometer combination. *Cem Concr Res.* 1972;2:16.

484 [17] McWhinney HG, Cocke DL, Balke K, Ortego JD. An investigation of mercury solidification and
485 stabilization in portland cement using X-ray photoelectron spectroscopy and energy dispersive
486 spectroscopy. *Cem Concr Res.* 1990;20:3.

487 [18] Sarott F-A, Bradbury MH, Pandolfo P, Spieler P. Diffusion and adsorption studies on hardened
488 cement paste and the effect of carbonation on diffusion rates. *Cem Concr Res.* 1992;22(2-3):439-44.

489 [19] Pihlajavaara SE, Pihlman E. Effect of carbonation on microstructural properties of cement stone.
490 *Cem Concr Res.* 1974;4(2):149-54.

491 [20] Villani C, Spragg R, Pour-Ghaz M, Weiss WJ. The Influence of Pore Solutions Properties on Drying in
492 Cementitious Materials. *J Am Ceram Soc.* 2014;97(2):386-93.

493 [21] Castro J, Lura P, Rajabipour F, Henkensiefken R, Weiss J. Internal curing: discussion of the role of
494 pore solution on relative humidity measurements and desorption of lightweight aggregate (LWA). *ACI*
495 *Special Publication.* 2010;270:89-100.

496 [22] Constantinides G, Ulm F-J. The effect of two types of C-S-H on the elasticity of cement-based
497 materials: Results from nanoindentation and micromechanical modeling. *Cem Concr Res.* 2004;34:14.

498 [23] Dri F, Jr. LGH, Moon RJ, Zavattieri PD. Anisotropy of the elastic properties of crystalline cellulose I β
499 from first principles density functional theory with van der Waals interactions. *Cellulose.* 2013;20(6):16.

500 [24] Dri FL, Shang S, Jr LGH, Saxe P, Liu Z-K, Moon RJ, et al. Anisotropy and temperature dependence of
501 structural, thermodynamic, and elastic properties of crystalline cellulose I β : a first-principles
502 investigation. *Modell Simul Mater Sci Eng.* 2014;22(8):1-28.

- 503 [25] Medeiros M, Helene P. Efficacy of surface hydrophobic agents in reducing water and chloride ion
504 penetration in concrete. *Mater Struct.* 2008;41:13.
- 505 [26] Mindess S, Young JF, Darwin D. *Concrete*: Pearson Education, Inc.; 2002.